Band 5 Polarization Assessment on *VY CMa* SV Observations

Draft v3

I. Martí-Vidal, W. H. T. Vlemmings, T. Carozzi

and rest of *Onsala's B5 busy week* Team

November 22, 2016

Contents

Name	Intent	EB (uid___A002_Xb978c3_ +)		
		X116b	X1955	X262a
J0522-3627	Flux/Polariz.	X	X	X
J2258-2758	Bandpass	X		
J0747-3310	Phase	X	X	X
J0725-2640	Check	X	X	X
VY_CMa	Target	X	X	X
J0635-7516	Bandpass			X

Table 1: Observed sources and their intents

1 Observations

The observations were taken on 16 October 2016, from 05:45 to 12:09 UT, with a gap at the middle of the observations (between 8:30 and 10:30 UT) due to the high elevation of the target. There was a total of 15 antennas participating in the observations. Two of these antennas (DV05 and DA58) were discarded, due to either too high system temperatures or bad-quality data.

There are five spws in this dataset: two centered around 183.5 GHz (spws 0 and 1), and three at around 172 GHz (spws 2, 3, and 4). Spws 0, 3, and 4 have narrow channel widths (244 KHz), furthermore spw 1 is very close to the water atmospheric line. Spws 1 and 2 have channel widths of 1.95 MHz and so are about 8 times wider than spw 0. Hence, the most logical approach is to calibrate spw 0 by transferring the gain solutions from spw 1. This includes solving for phase (through an extra gain table) and amplitude (through non-normalised bandpass tables using provided bandpass calibrator fluxes) offsets between the spectral windows. Regarding spws 3 and 4, the signal from the calibrators is strong enough for a successful calibration without transferring phase solutions from spw 2. The list of spectral windows is given in Table 2.

The list of observed sources is given in Table 1. There were a total of three execution blocks. The observations to calibrate the bandpass are deliberately not observed in the second EB (ALMA session mde), and the bandpass calibrators on the first and last EBs are different, and the one in the first EB of poorer quality. Due to these limitations, we decided to perform the a priori calibration (i.e., WVR, Tsys, and antenna-positions) on each EB separately, but then concatenate the three EBs for the rest of the calibration, in order to optimize the calibration using the joint information from all three EBs.

SPW	Chan 0 (GHz)	Chan. Width (MHz)	Num. Chan	Total BW (GHz)
0	183.1817	0.244	960	0.2344
1	183.9461	1.953	960	1.8750
2	171.9360	-1.953	960	1.8750
3	172.5291	-0.244	480	0.1172
4	173.7360	-0.244	480	0.1172

Table 2: Observed spectral windows

2 A priori calibration

The WVR solutions for the first run (i.e., X116b, see Table 1) show a remarkable phase drift on the observations of the bandpass calibrator for antennas DA49 and DV12 (see Fig. 1). We notice that the source is setting (Fig. 2, left) and that its azimuth is close to the baseline direction between these two antennas (Fig. 2, right). We suspect that this phase drift may be related to artifacts (shadowing? cross-talk between radiometers?) related to this baseline, so we decided not to apply the WVR solutions for the bandpass calibrator.

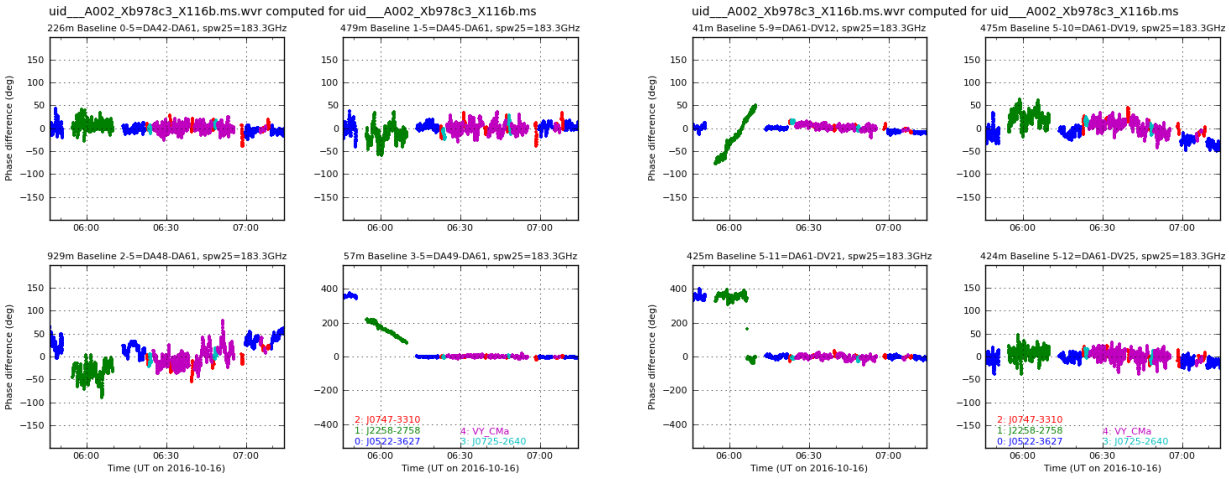

Figure 1: WVR phase solutions for baselines related to DA61. Notice the drift of the bandpass calibrator (green) on DV12 and DA49. The slopes are exactly the same, so that the effect of the drift on the baseline DA49-DV12 is cancelled, whereas it appears on any other baseline related to either DA61 or DV12.

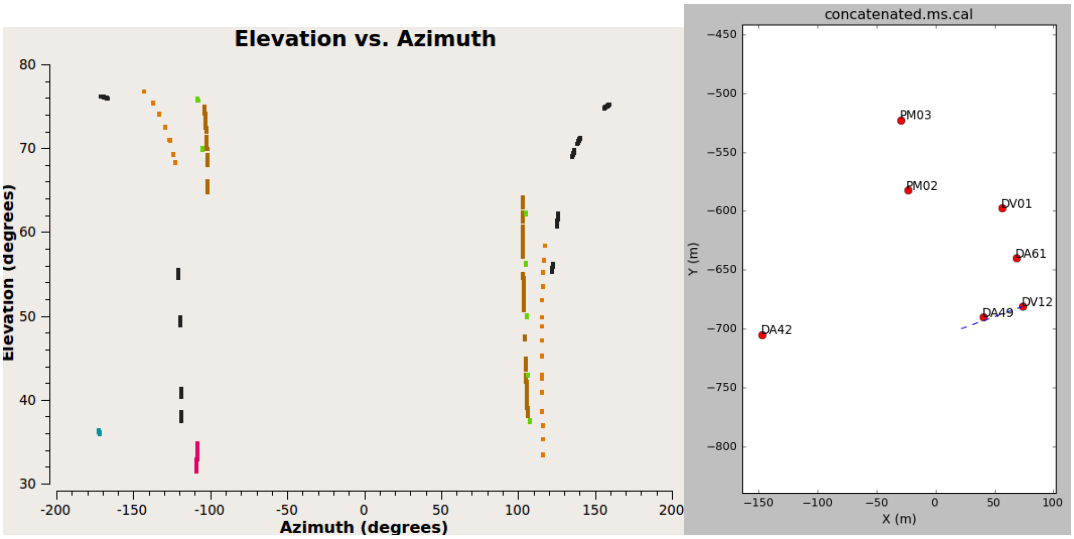

Figure 2: Left, source elevation vs. azimuth. The bandpass calibrator in the first EB is shown in magenta. The source is setting, and its azimuth is ~ -110 deg.. Right, the inner part of the array distribution. The dashed line points in the direction to the bandpass calibrator, which is roughly aligned to the baseline DA49-DV21.

3 Ordinary calibration

3.1 SetJy

As it will be needed to derive the amplitude corrections of the spectral windows relative to each-other in preparation for the gain transfer between spw1 and spw0, we derive the fluxes of the bandpass calibrators using an initial normal calibration run of spw1-4. The derived values (1.575 Jy and 0.895 Jy at 177 GHz for J2258-2758 and J0635-7516 respectively and manually inserted using `setjy`.

3.2 Bandpass

We show the pre-bandpass gain solutions (i.e., gain vs. time) for antennas DA42 and DV01 in Fig. 3. We notice the low SNR in spw 0, with more than a half of solutions failed. It is thus mandatory to apply the phase-transfer calibration from spw 1. To perform the phase transfer, we derived the phase offset between the two spectral windows. We basically ran `gaincal` (with `solint='inf'` and `combine='scan'`) on spw 0, by applying (on-the-fly) the pre-bandpass phase gains from spw 1. This phase-offset is then applied to spw 0, so that the solutions on spw 1 can be transferred to this window at each integration time (not only for the pre-bandpass, but also for the remaining of the gain calibration).

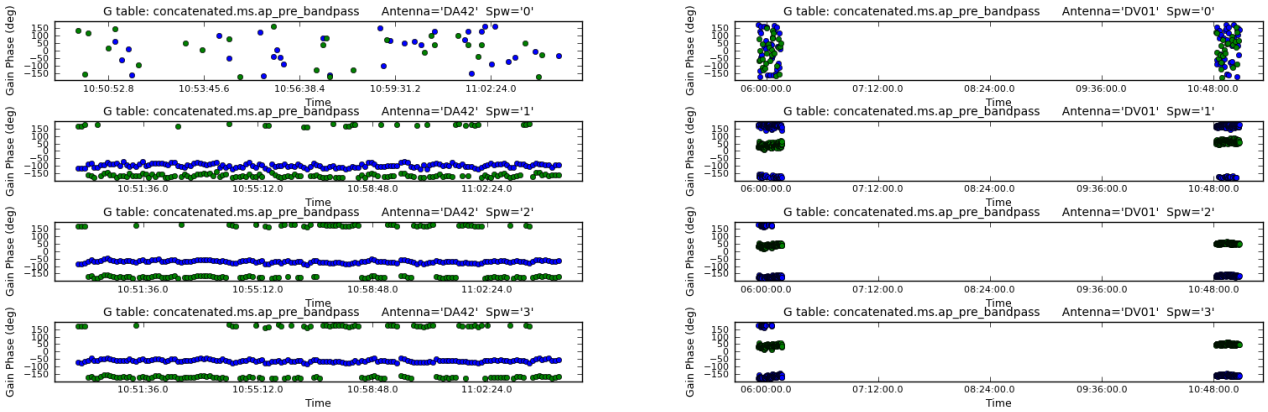

Figure 3: Pre-bandpass gains for antennas DA42 (which was not observing during the first EB) and DV01. Notice the poorer quality and high failure rate for spw 0.

We combine the two bandpass observations (i.e., the bandpass scans in the first and last EBs, see Table 1), to increase the SNR of the BP gains. Hence, `bandpass` is run with `combine='scan,field,obs'`. To properly transfer the amplitudes we do not normalize the solutions, setting `solnorm = False`. Even using the two bandpass scans and transferring the phase gains from spw1 to spw0, there is a high failure rate (about 90%) in the bandpass solutions for spw 0. We need thus to average over a large number of spectral channels per BP solution in spw 0, in order to get enough signal for a successful bandpass calibration. We have used `solint='inf,200ch'` for spw 0 (i.e., the BP table only has 5 channels across the spectral coverage of spw 0). We show an example bandpass gain in Fig. 4.

3.3 Phase gains

We show example phase gains (with one solution per scan) in Fig. 5. The reference antenna is DV12. We notice the phase jumps at the reference antenna in spw 0. This is due to failed solutions at this antenna for a subset of scans, which force CASA to re-reference the phase gains to alternative reference antennae. These jumps would spoil the full-polarization calibration, since a time dependence of the X-Y cross-phase would be introduced.

Since there are no jumps in the other spectral windows, we decided to transfer the phase, again, from spw 1 to spw 0, in order to allow us to perform a full-polarization calibration on spw 0.

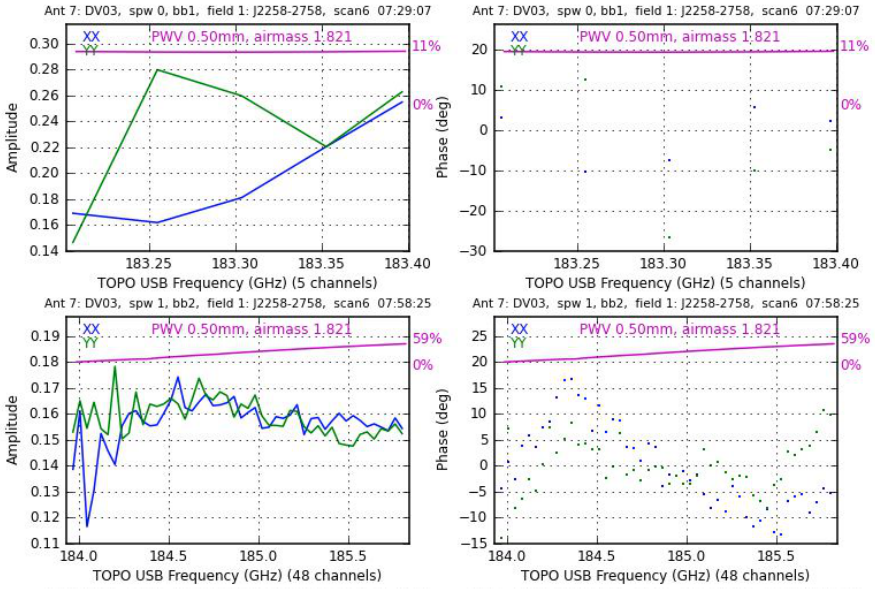

Figure 4: Bandpass gains for antenna DV03 in spws 0 and 1.

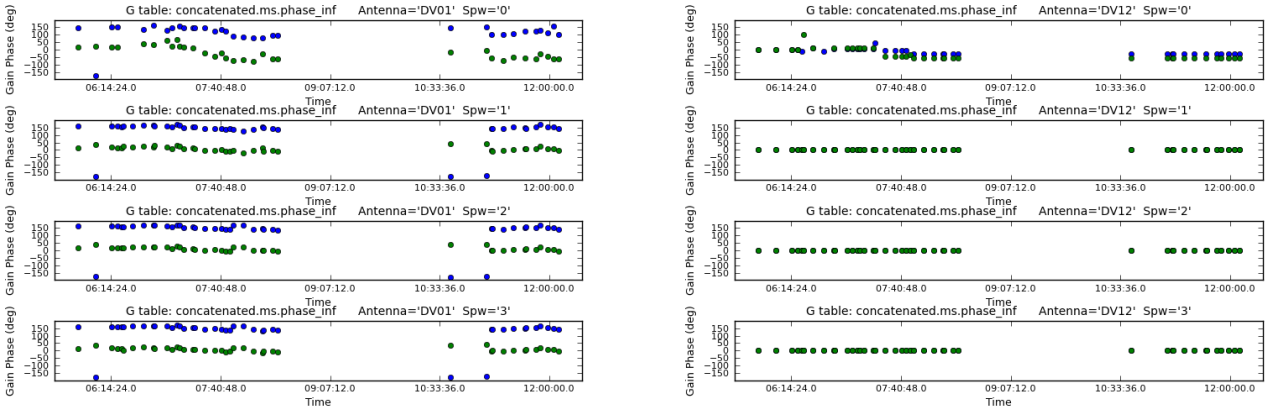

Figure 5: Phase gains for antennas DV01 (left) and DV12 (reference antenna, right). Notice the phase jumps in DV12 for spw 0.

3.4 Amplitude gains

We show example amplitude gains in Fig. 6. We notice that the amplitude gains for spw 0 differ from those at the other spectral windows, especially during the observations of the bandpass calibrator in the first EB. This may be related to an enhanced atmospheric opacity close to the water line, which would introduce higher effects at lower elevations. Since spw 0 is remarkably noisier than spw 1 (the bandwidth is about 8 times narrower), we decided to not use the noisier amplitude gains derived for spw 0, and apply the amplitude gains from spw 1 instead.

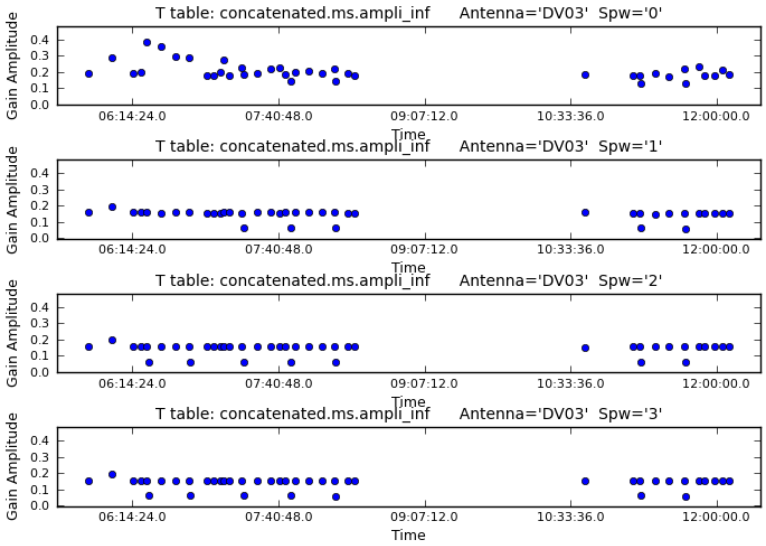

Figure 6: Amplitude gains for antenna DV03.

4 Polarization calibration

4.1 Gain ratios and QU of polarization calibrator

We show the gain ratios on the polarization calibrator (i.e., the amplitude gains solved in 'G' mode) in Fig. 7 (left). The fractional polarization of the calibrator, derived from these gain ratios is $\sim 3.2\%$. It is a relatively low polarization intensity, although the combined solution for all antennas seems to still be good enough for the calibration, judging from the small scatter in the estimate of Q and U among the spectral windows (Table 4.1). Since the X/Y gain ratios have to be applied to the data for an optimum leakage calibration, we have to include spw 0 in this second run of `gaincal`. However, using `solint='int'` results in a large set of failed solutions for spw 0. Hence, we decided to run the 'G'-mode `gaincal` with `solint='inf'`, which should not affect the slow dependence of the gain ratio on parallactic angle, needed to derive the calibrator's polarization. The Stokes Q and U estimated from the Gx/Gy gain ratios are shown in Table 4.1). The self-consistency across spws (indicative of a robust estimate of the true Q and U parameters of the calibrator) is clear.

4.2 Cross-hand phase

The X-Y cross-phase of spw 0 could eventually be derived from that of spw 1 plus the offsets between spw 1 and 0, derived during the ordinary phase calibration (Sect. 3.2). However, this

SPW	Gx/Gy	Q (Jy)	U (Jy)	p/I	PA (deg.)
0	0.97865	-0.03196	-0.01682	0.03612	-76
1	0.99217	-0.02955	-0.01454	0.03293	-76
2	1.00388	-0.02552	-0.01466	0.02943	-75
3	1.00234	-0.02724	-0.01410	0.03068	-76
4	1.00787	-0.02583	-0.01502	0.02988	-75

Table 3: Fitted polarization of calibrator, obtained from the Gx/Gy gain ratios.

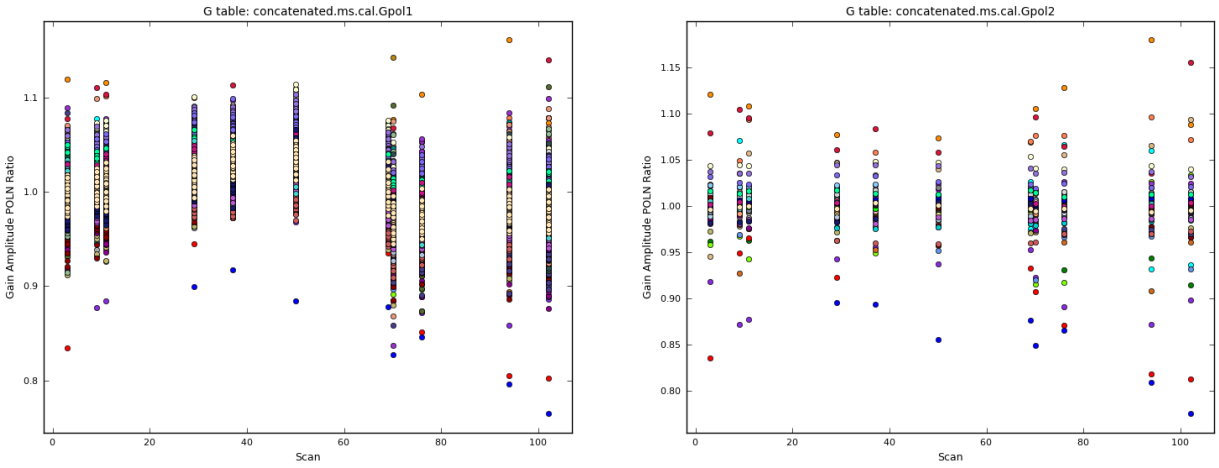

Figure 7: Left, Gx/Gy amplitude gain ratios for all antennas observing the polarization calibrator. Spw 0 is shown in blue. Right, Gx/Gy ratios using the estimated calibrator's polarization.

approach would deviate from the current calibration strategy for full-polarization observations. We have instead decided to derive the X-Y cross-phase of each spectral window without any phase transfer from neighbouring windows.

If we solve for one solution per channel, the results for spws 0 and 1 are not correct (Fig. 8, left). Jumps of 90 and 180 deg. appear accross the spws (in spw 1, the jumps start to appear at the lower frequencies, close to the water line). Hence, we have to pre-average frequency channels to find the solutions, in a similar way as we did for the bandpass calibration. We have pre-averaged 20 channels in spw 1 and 200 channels in spw 0. With this frequency averaging, the phases do not show jumps accross the bandwidth (Fig. 8, right). We notice that the X-Y phase difference between spws 0 and 1 (which should be either zero or 180 deg.) is about 200 deg. or more. A phase difference between spw 0 and 1 at the reference antenna (which would not be reflected in the phase-transfer calibration table derived during the ordinary calibration) would explain such a phase difference between the X-Y cross-phases of spws 0 and 1. Obviously, the

alternative approach that we propose, in the previous paragraph, to calibrate the X-Y phase of spw 0 (using phase-transfer from spw 1) would still work in that case.

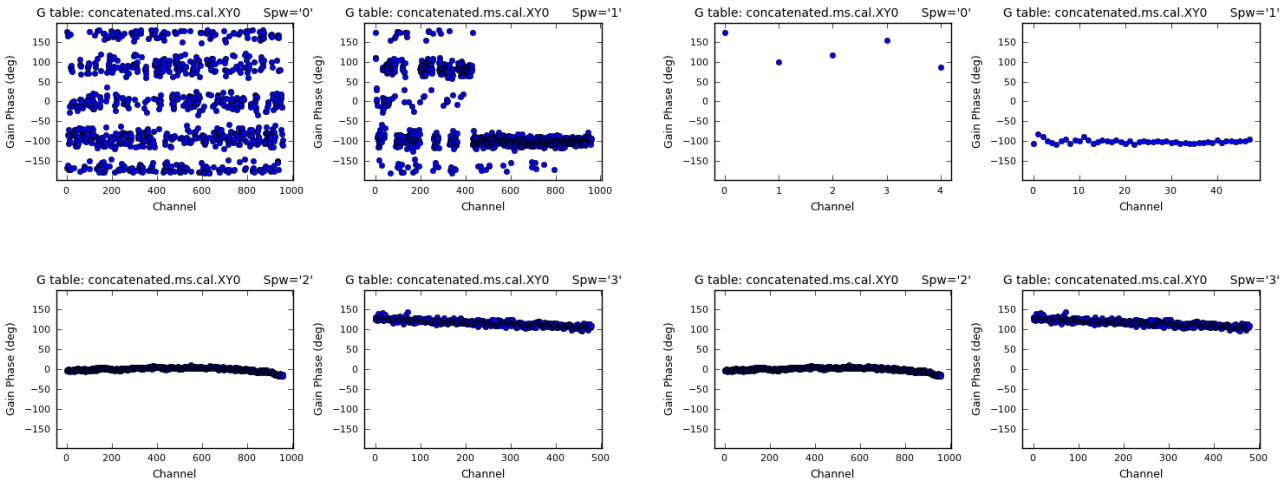

Figure 8: X-Y cross-phases at the first 4 spectral windows. Left, with no channel averaging. Right, with a heavy channel averaging (200 channels for spw 0 and 20 channels for spw 1).

At the time of writing the report the "almahelper" function xyamb seems to have a bug when dealing with X-Y cross-phase tables generated with the "append" option of gaincal, as it is shown in Fig. 9 (CAS-9360). The "append" operations are needed when a different channel averaging is used for the different spws. The function seems to only use the estimated QU of spw 0 to derive the phase ambiguities, being unable to read the gains coming from the "append" operations of `gaincal`. In addition to this, we have found problems when running `polcal` with an on-the-fly application of the cross-phase tables generated with the `append=T` keyword of `gaincal`. We have overcome all these issues by calibrating each spw in independent steps, saving different calibration tables per spw.

4.3 D-terms

The best estimate of the calibrator's polarization is given by the average of the QU estimates from the Gx/Gy gain ratios of spws 1 to 4 (Sect. 4.1). The average fractional polarization of the model is 3.2%. Using this model as a priori in a second run of `gaincal` (and adding parallactic-angle correction) gives us a set of new Gx/Gy gain ratios, from which a residual polarization of 0.24% (average for spws 1 to 4) and 0.79% (for spw 0) is found (see Fig. 7, right). We find this residual signal acceptable (at least for spws 1 to 4), considering that the leakage has not been calibrated yet at this stage.

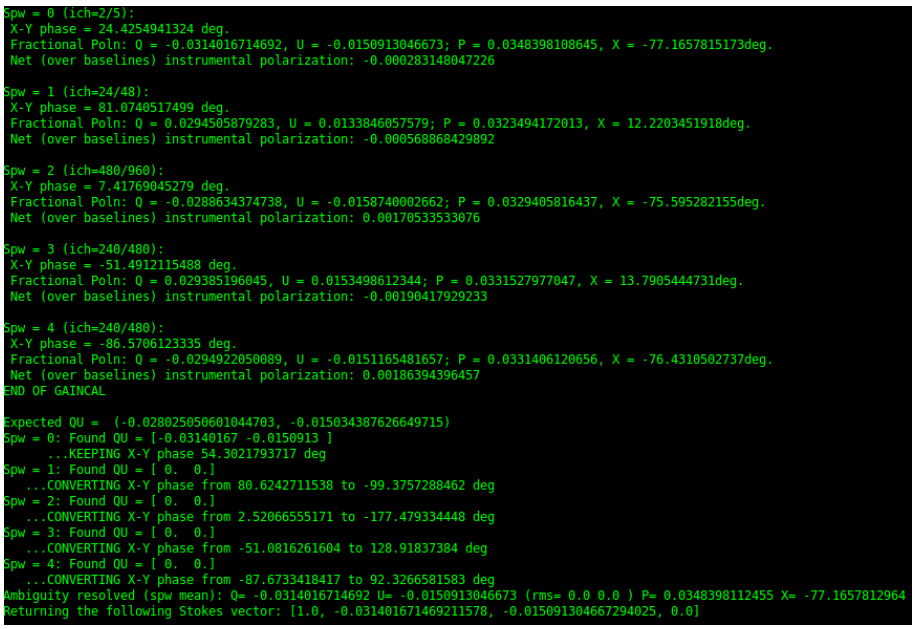

Figure 9: Output of the calibration script at the stage of `xyamb`. Notice the zeros in the estimated QUs, used to figure out the phase amiguities in spectral windows 1 to 4.

The D-terms are determined using the calibrator's polarization model and the same channel averaging that was used for solving the X-Y cross phases in spws 0 and 1. We applied an additional 20-channel spectral averaging to the other two narrow spectral windows (spws 3 and 4), to increase the SNR in the cross-hand correlations. The resulting D-terms are shown in Fig. 10 (spws 0 and 1, close to the water line) and Fig. 11 (spws 2, 3, and 4). The values are of the order of a few %, with the exception of the channels close to the water line, where the real part of the D-term estimates are as high as 20%, being evenly distributed around zero (X in one side and Y in the opposite side). This behaviour in the real parts of the D-terms is typically found in cases where the model values of the calibrator's Stokes Q and U are not correct. However, we have used the very same calibrator model for all spws and, besides this, the estimated Q and U of the calibrator, based on the XX and YY gain ratios, is self-consistent among spws (Table 4.1). The D-term values for spws 0 and 1 are likely affected by a higher noise related to the atmospheric opacity close to the water line (see Sect. 4.3.1). The polarization images close to the water line should hence be taken with care.

In any case, we notice that the images of Stokes Q and U are insensitive (in a first-order approximation) to any real part of the D-terms that is symmetric between D_x and D_y (i.e., to any real value R such that $D_x \rightarrow D_x + R$ and $D_y \rightarrow D_y - R$). Such a value R would map into artefacts in Stokes V (in a first-order approximation of the leakage, i.e., up to values $\sim I \times |D|$), but not in the other Stokes parameters. Given that the real parts of the D-terms in spws 0 and

1 are roughly distributed in a symmetric way (see Fig. 10, where colors represent antennas) the images of Stokes Q and U should *only* be affected by leakage up to *second-order* corrections (at the level of $\sim I \times |D|^2$ and/or $p \times |D|$).

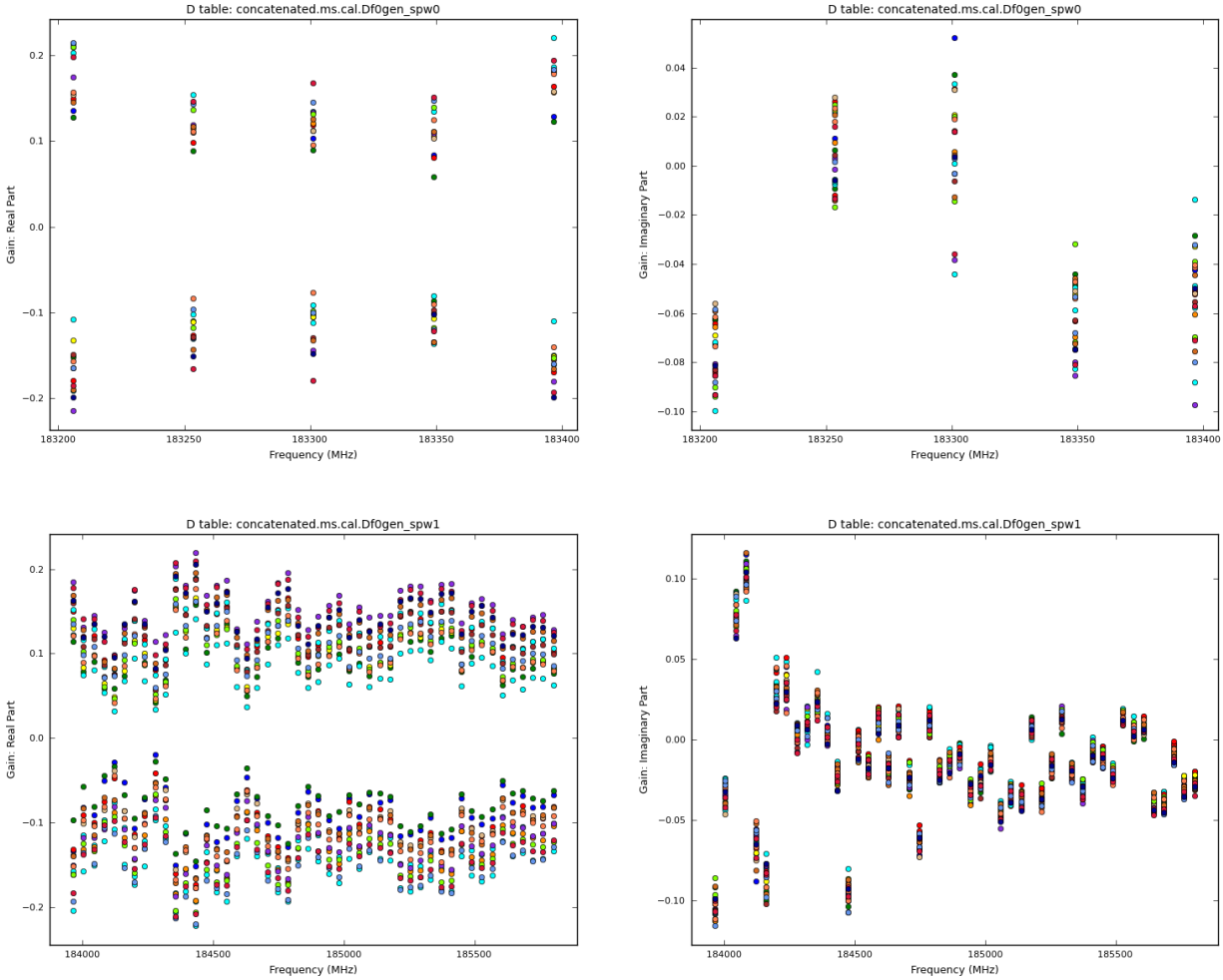

Figure 10: Dterms for the first two spectral windows. Channel averaging has been used for spws 0 (200 channels per solution) and 1 (20 channels per solution).

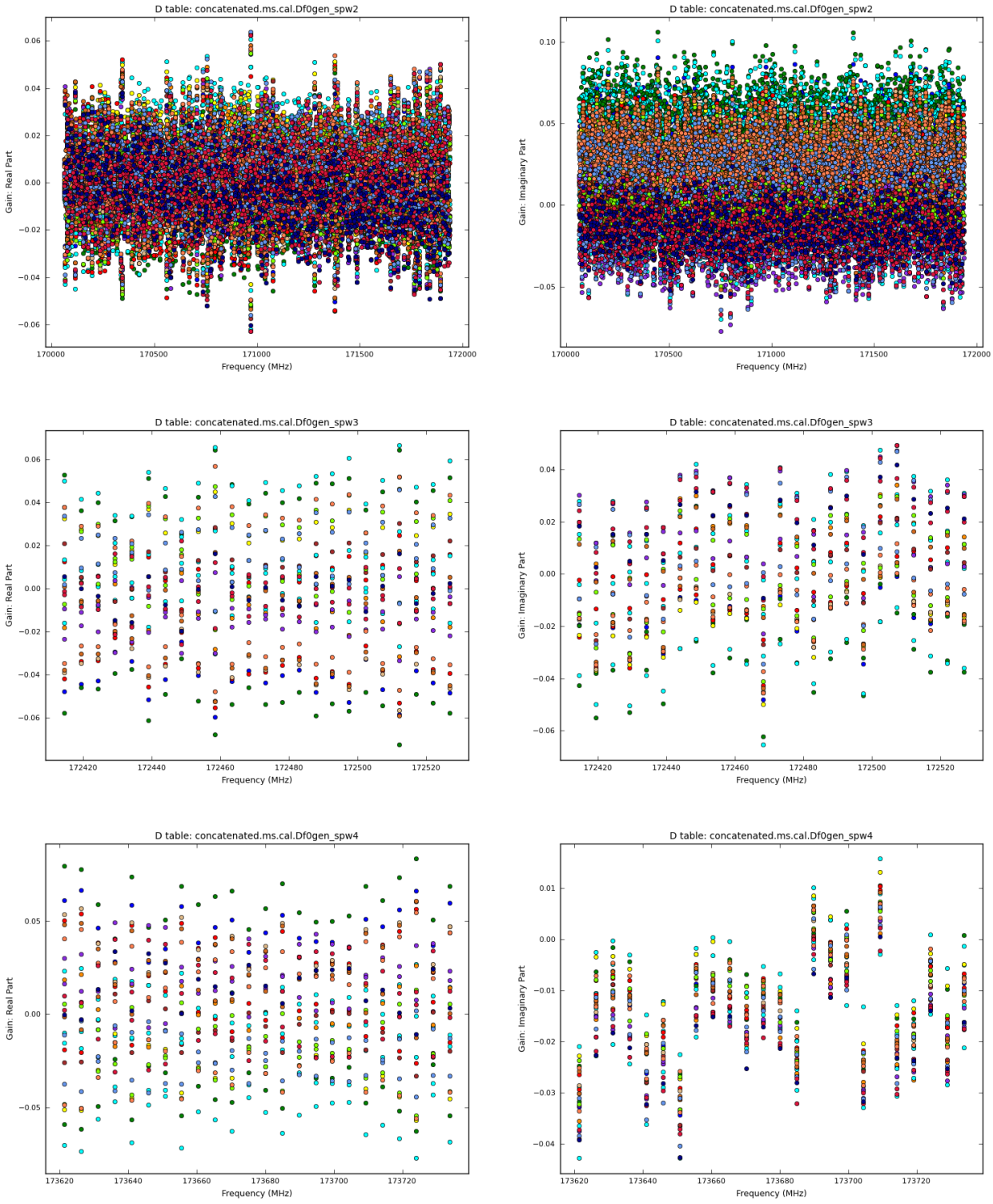

Figure 11: Dterms for spectral windows 2 to 4. Channel averaging has been used for spws 3 and 4 (20 channels per solution).

4.3.1 Effect of water absorption on the polarization calibration and images

The XY visibilities of the polarization calibrator, for baseline $A - B$, are

$$XY = U' + XX\,(D_y^B)^* + YY\,D_x^A + jV, \tag{1}$$

where U' is Stokes U measured in the frame of the antenna mounts (i.e., it depends on the parallactic angle) and D_i^A is the (complex) Dterm of antenna A in the polarization channel i. Working out this equation, we have

$$XY = U' + I\,(D_x^A + (D_y^B)^*) + Q'\,((D_y^B)^* - D_x^A) + jV \tag{2}$$

where Q' is Stokes Q measured in the frame of the antenna mounts. For the YX visibilities, we have a similar expression,

$$YX = U' + I\,(D_y^A + (D_x^B)^*) + Q'\,(D_y^A - (D_x^B)^*) - jV. \tag{3}$$

If the data are well calibrated in amplitude, for the two polarization channels, and the calibrator is strongly polarized, D_x^A and D_y^B can be derived from Eqs. 2 and 3. However, if the polarization level of the calibrator is very low (compared to the noise), the terms containing Q' (in Eqs. 2 and 3) may not be well constrained by the fit, so that the fitted Dterms can be affected in the way $D_x^A \rightarrow D_x^A + R$ and $D_y^B \rightarrow D_y^B - R$, being R a real number, common to the Dterms fitted for all the antennas. Adding R to the Dterms in this way leaves the terms containing I (in Eqs. 2 and 3) invariant.

If the amplitude calibration of XX and YY is not correct, its deviation from the true gains may be absorbed in the terms containing Q' (Eqs. 2 and 3), which would also introduce an undesired R into the Dterms. This is specially true if the amplitude deviation depends smoothly on the antenna elevation (i.e., if it depends, indirectly, on parallactic angle). In Fig. 12, we show the calibrated amplitudes of the polarization calibrator in spw 1, but divinding the spectral window in two chunks (i.e., one half closer to the water line and the other half farther away from the line). It can be clearly seen that the water absorption (which is a function of the antenna elevations, via the atmospheric mapping function) is introducing a systematic bandpass change throughout spw 1, which is then absorbed by the Q' terms (Eqs. 2 and 3) during the polarization calibration. This also helps explain the higher dispersion in the imaginary part of the Dterms for the lower channels in spw 1 (see Fig. 10).

We notice that the systematic bandpass effect has the same sign for XX and YY (i.e., magenta is over black at low elevations in both polarizations, see Fig. 12). This is an expected

effect, since the atmospheric absorption is independent of the polarization. Indeed, such a polarization-independent amplitude bias will affect XY and YX in a way consistent with the same sign of Q' (see Eqs. 2 and 3), so that the same R (and $-R$) can be consistently added to all the D_x (and D_y) Dterms, in a self-consistent fit to the XY and YX visibilities.

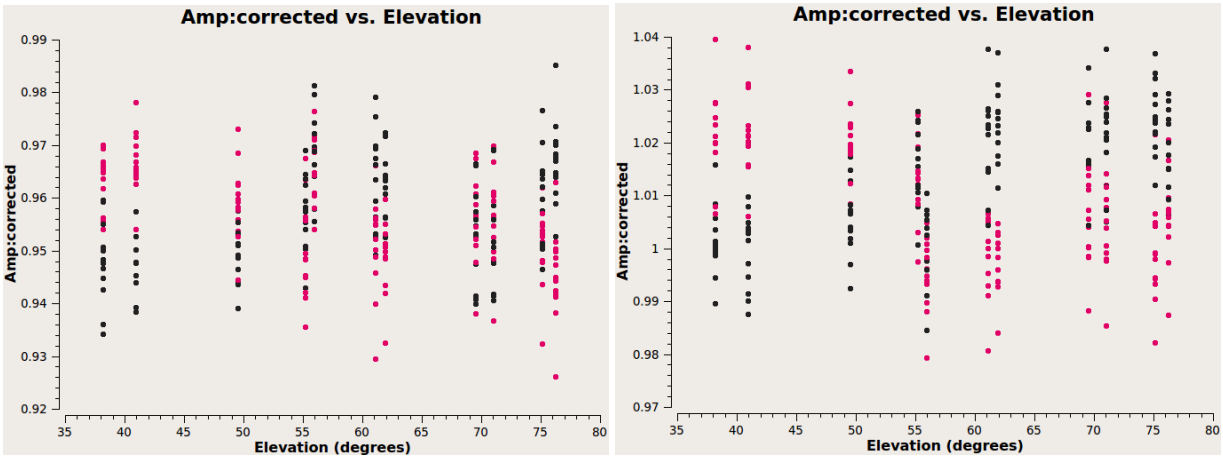

Figure 12: Calibrated amplitudes in spw 1 for the polarization calibrator, in XX (left) and YY (right), averaged between channels 0−480 (black) and 481−960 (magenta). All data are shown. A per-antenna averaging has been applied.

4.3.2 Dealing with the vapour mapping function

One way of removing the effect of elevation-dependent atmospheric absorption profile (i.e., the mapping function of the water vapour) is to solve for the bandpass at each different elevation. This bandpass can be understood as a "second-order bandpass calibration", to account for changes in the atmosphere (i.e., not for insturmental effects, which are completely modelled in the ordinary bandpass table). We can use the phase calibrator to derive a bandpass solution every 15 minutes using a coarse channel averaging of one solution every 100 channels (in order to have enough SNR per solution). This second-order bandpass shall be computed by pre-applying the ordinary bandpass plus the "int"-based phase gains. Since the target is not far from the phase calibrator, the bandpass solutions derived from the calibrator should also be valid for the target (the elevations of both sources should be similar in all the scans). However, we need to derive an independent bandpass solution for the polarization calibrator, given that the antenna elevations may differ substantially between the phase calibrator and the polarization calibrator.

Ideally, we should combine the two polarization channels, XX and YY, when deriving these bandpass solutions (since the mapping function does not depend on polarization), but CASA does not offer such a feature in its current version.

We call the new bandpass tables "uid*.atmosphere", and apply them together with the ordinary bandpass table. After applying this new table, the calibrated amplitudes in spw 1, for the polarization calibrator, are shown in Fig. 13. This figure does not show the systematic amplitude difference between the two halfs of spw1, although the first scan is now missaligned with the others. The real part of the new Dterms decreases in general (although it *increases* in some cases, Fig. 14), but the overall improvement is not very big. Indeed, far from the water absorption, the real part of the Dterms is almost unchanged.

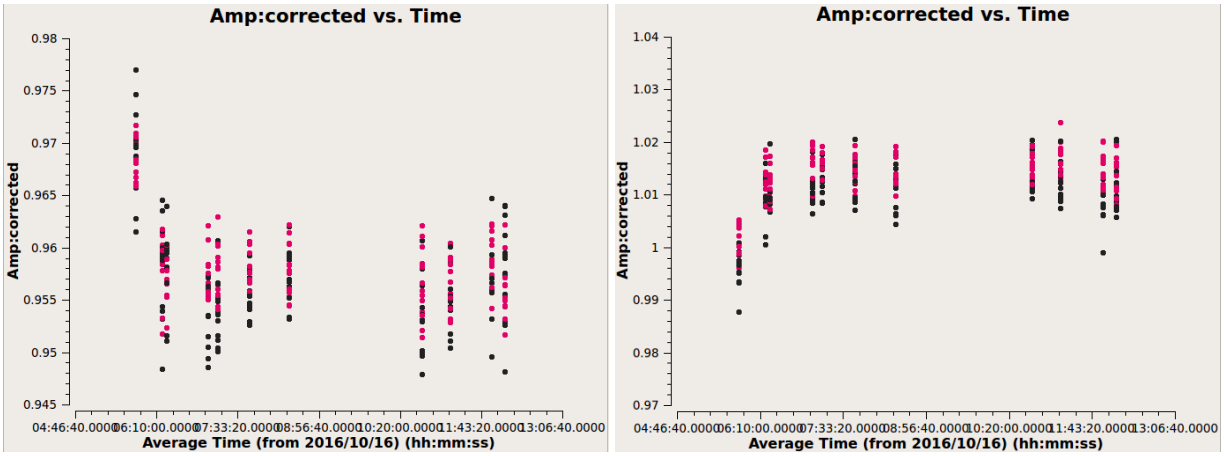

Figure 13: Same as in Fig. 12, but applying a correction for the elevation-dependent water-vapour absorption.

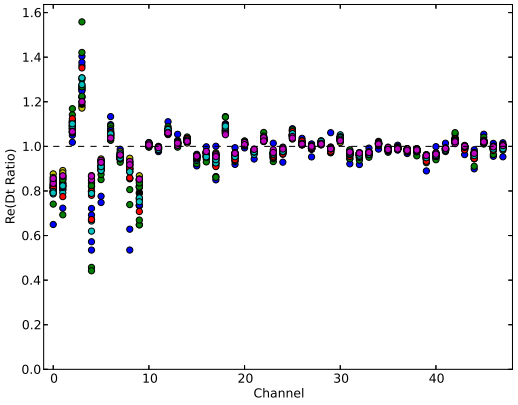

Figure 14: Ratios between the real part of the new Dterms (i.e., after applying the mapping-function correction) and the real part of the original Dterms.

4.4 X/Y amplitude ratios for all observations

The X/Y amplitude ratios for each antenna, derived using the calibrator's polarization model as a-priori (and pre-applying the X-Y cross-phases and Dterms) are shown in Fig. 15. The

values found are within the typical expected amplitude ratios (i.e., X-to-Y amplitude differences within 10%). These amplitude ratios are applied to the whole dataset, together with the rest of calibration tables, and the calibrated data are finally split for imaging.

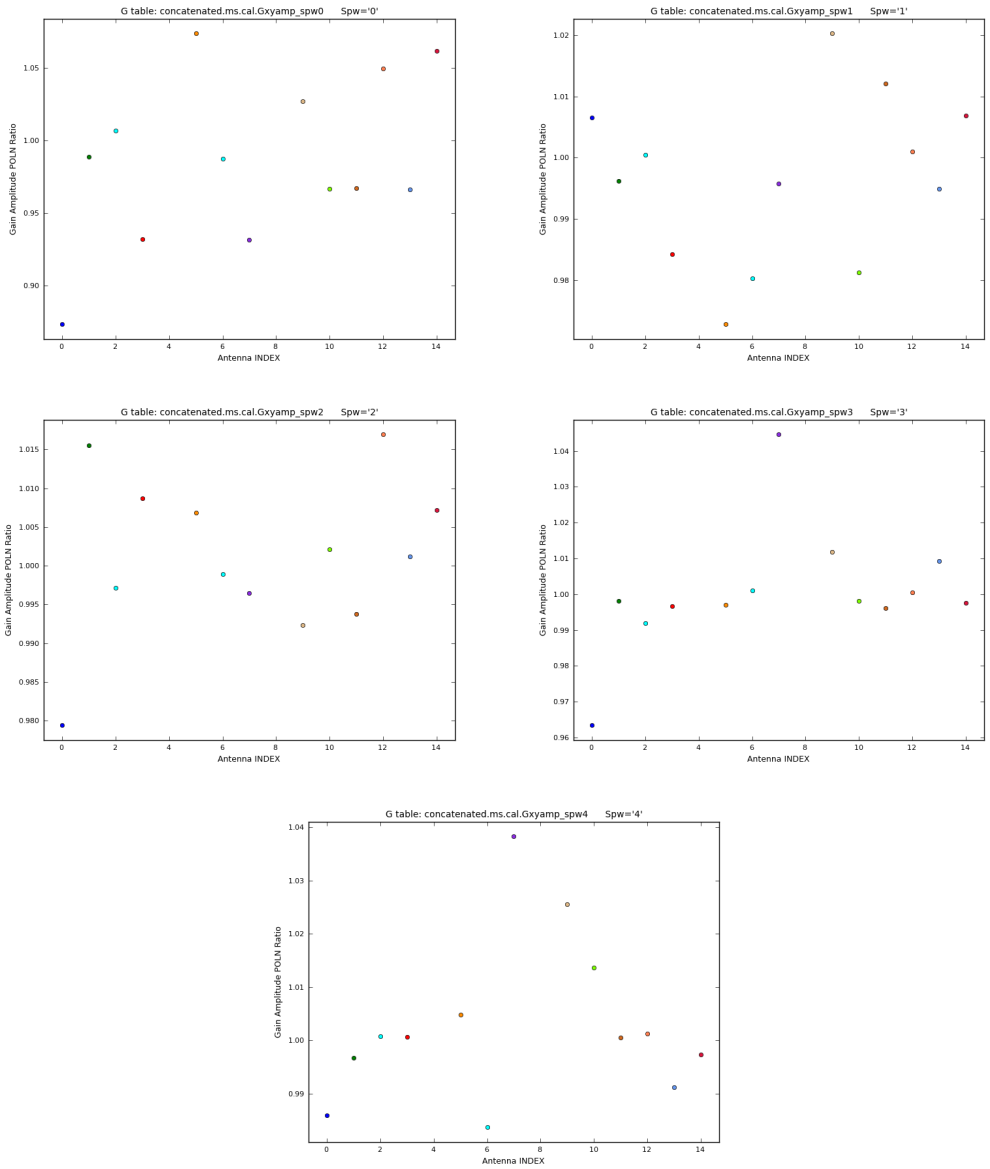

Figure 15: Gx/Gy constant amplitude ratios as a function of antenna index, accounting for the calibrator's polarization and instrumental leakage.

5 Imaging

5.1 Calibrators (continuum)

We have imaged (in continuum mode) the Stokes I, Q, U and V of the polarization and phase calibrators, as well as the check source (see Table 1). The spws 0, 1, and 2 have been imaged

independently, to check for possible systematics related to the leakage calibration (Sect. 4.3). In all the following images, we have used the `clarkstokes` mode in CLEAN, with a pixel size of 0.025 arcsec and an image size of 1024×1024 pixels. The visibility-weighting scheme for all the images has been set to `natural`.

5.1.1 Polarization calibrator

The images of the polarization calibrator are shown in Fig. 16 for spws 0, 1 and 2. The root-mean-square, RMS, of the residuals in each Stokes parameter is given in Table 4. The images in spw 0 are noisier than those in spws 1 and 2, being spw 2 the most sensitive for all Stokes parameters. This is an expected result, since spws 0 and 1 suffer from the higher atmospheric opacity close to the water line. For Stokes I, the image in spw 1 is 1.58 times noisier than spw 2; for Stokes Q and U, the rms ratio is as high as 5.52 and 6.06, respectivetly. The lower RMS ratio in Stokes I can be understood in terms of a partial dynamic-range limitation that would affect both spws, 1 and 2. This limitation would not affect the (more compact) polarized emission, so that higher rms ratios are obtained for Q and U. For Stokes V, the image in spw 1 is about 10 times noisier than in spw 2. This higher RMS ratio can be understood as the effect of the symmetric real-part of the Dterms in spw 1 leaking into Stokes V (see Sect. 4.3). For the case of spw 0, the thermal noise is the main limitation for all Stokes parameters.

The images of the polarization calibrator are self-consistent between spws 0, 1 and 2 (Fig. 16). This gives us confidence on the polarization calibration of spws 0 and 1, even accounting for the pathological behavior in the real parts of the D-terms. As we have already noticed in Sect. 4.3, such symmetrically distributed real parts of the D-terms would not affect Stokes Q and U (at a first-order approximation of the leakage). Indeed, a wider image of the calibrator (Fig. 17) reveals a polarized hot spot in the SE direction, which shows the same polarization angle and intensity in the images of spw 1 and 2.

5.1.2 Phase calibrator

The continuum images of the phase calibrator, for spws 0, 1 and 2, are shown in Fig. 18. The polarization fraction is very low (about 0.5%, from the image at spw 2). The only spw where a clear polarization signal is detected is spw 2, where the polarization vectors are ordered across the source peak. In the other windows (spw 0 and 1), the polarization vectors look random. We show the rms of the image residuals, for each spw, in Table 5. The images are clearly limited by thermal noise for all Stokes parameters in spws 0 and 1, whereas Stokes I suffers

SPW	I	Q	U	V
	(mJy/beam)			
0	1.27	1.22	1.25	1.51
1	0.30	0.21	0.20	0.44
2	0.19	0.038	0.033	0.043
1/2	1.58	5.52	6.06	10.2

Table 4: Residual rms of the polarization calibrator (using natural weighting) for spws 0, 1, and 2. The last row shows the rms ratio between spws 1 and 2.

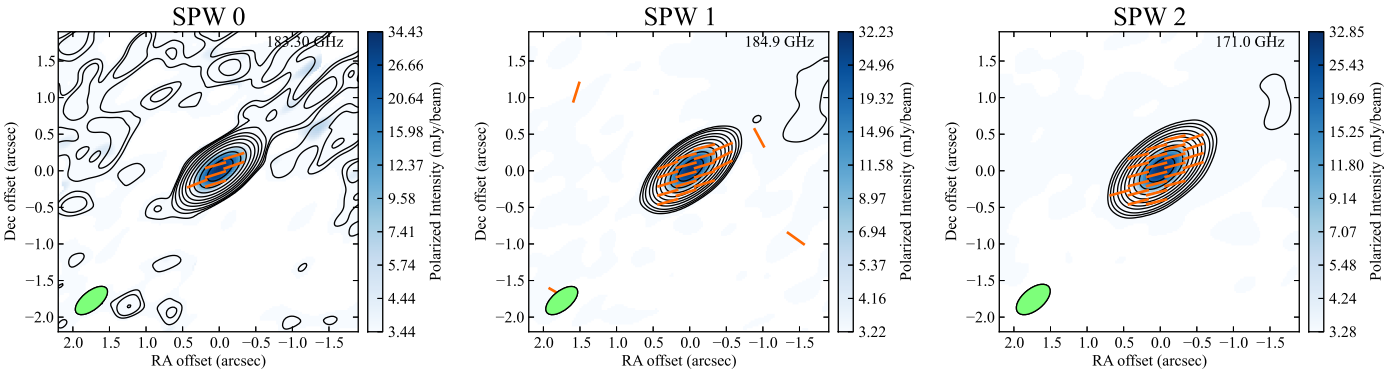

Figure 16: Full-polarization images of the core of the polarization calibrator in spws 0, 1 and 2. The contours show total intensity and are set at 0.1, 0.2, 0.4, 1, 2, 4, 8, 16, 32 and 64% of the intensity peak. The cutoff of the polarization lines is set to 2% of the polarization peak (for spws 1 and 2) and to 25% of the polarization peak (spw 0).

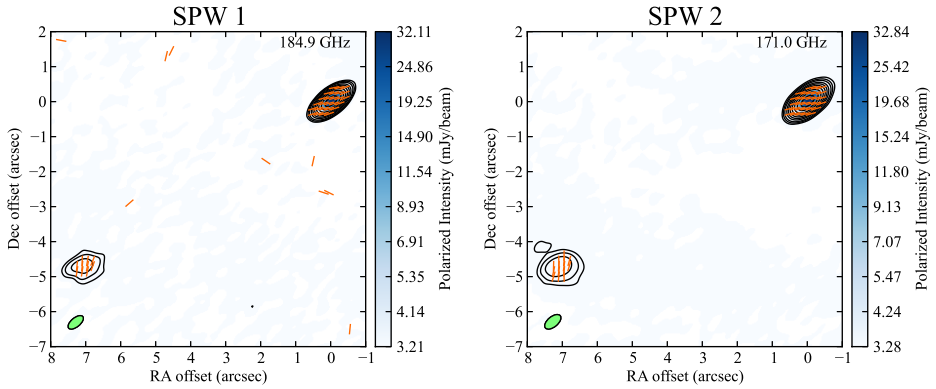

Figure 17: Same as in Fig. 16, but for spws 1 and 2, and showing a wider sky coverage.

from dynamic-range limitation in spw 2. The most sensitive spw is again spw 2. We notice that the peak polarization in each image is biased by the thermal noise in Stokes Q and U.

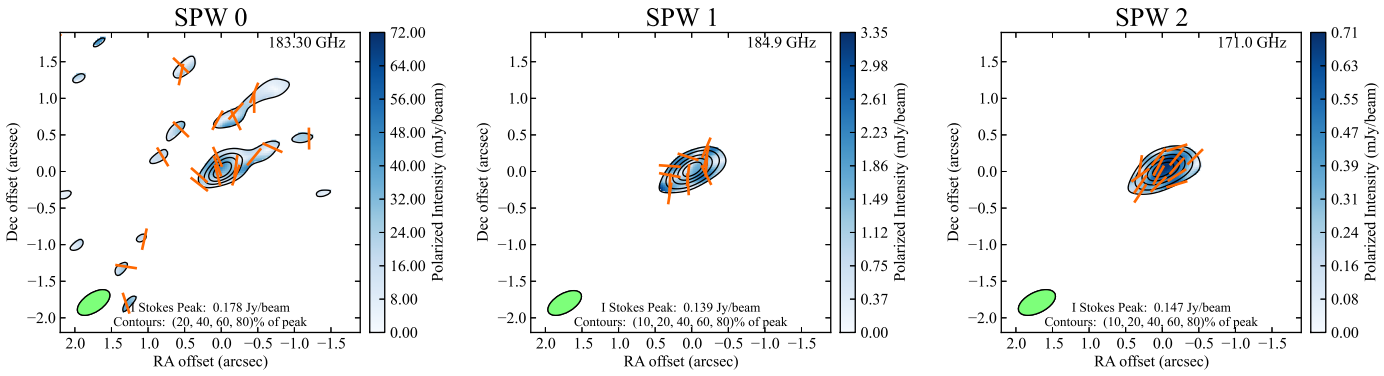

Figure 18: Full-polarization images of the phase calibrator in spws 0, 1 and 2. The contours show total intensity. The cutoff of the polarization lines is set to the contour cutoff.

SPW	I	Q	U	V
	(mJy/beam)			
0	12	11	12	12
1	1.9	1.5	1.5	1.5
2	1.5	0.2	0.2	0.2

Table 5: Residual rms of the phase calibrator (using natural weighting) for spws 0, 1, and 2.

5.2 Target

As the target of the observations are strong SiO and H_2O masers around VY CMa, we can use the masers to perform self-calibration. We first prepare the data by performing `mstransform` to align all channels in the proper radio-LSR reference frame. We then perform a continuum subtraction, basing the subtraction on the channels sufficient far from the atmospheric window. The primary self-calibration is done, in phase (integration based) and amplitude (30 sec intervals) on one of the compact SiO maser channels in spw 3 (see Fig.19). The self-calibrations improves the dynamic range from 167 to 4135. A big part of this improvements comes from the amplitude self-calibration, where it is noticed that one of the antennas (DA61, shown in Fig. 19) requires a significant correction in a short timerange. After the self-calibration, a new continuum subtraction is performed. It is noted that the transfer of self-calibration solutions in spw 3 to the H_2O in spw 3 is sub-optimal. Hence, further phase and amplitude self calibration is performed on a strong H_2O maser channel. This increases the dynamic range significantly, although it is clear that the strong maser channels will remain dynamic range limited.

In Table. 6 we list some representative rms values compared to the expected values based on

SPW	I	OT
	(mJy/beam)	
0	50	36
3	3.4	4.2
cont	0.2	0.2

Table 6: Residual rms of the target compared to OT values.

OT calculations. Spw 3 and the continuum clearly reach the expected noise level (in line free window in case of spw 3). Spw 0 is still somewhat too high, though this value is very sensitive to the exact atmospheric conditions.

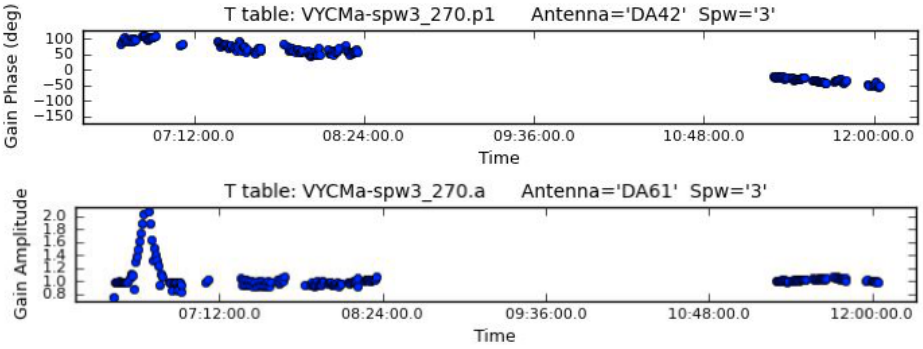

Figure 19: Examples of the self-calibration solutions for Phase (top) and amplitude (bottom).

5.2.1 Target (continuum)

Continuum imaging is done using the least noise part of spw 1 and the line-free parts of spw 2,3, and 4. The image is shown in Fig. 20 and shows the structure expected based on the previous ALMA band 7 and 9 SV observations. Imaging was performed using Briggs weighting resulting in a 0.49×0.23" beam.

5.2.2 Spectral cubes (spws 0, and 3)

The SiO spw3 is imaged in full polarisation and results are shown in Fig. 21. Imaging was performed using Briggs weighting resulting in a 0.50×0.23" beam. The H_2O spw is only imaged in Stokes I, considering the possible problem with the polarisation calibration within the atmospheric window. Moment maps are shown in Fig. 20. Imaging was performed using Briggs weighting resulting in a 0.47×0.23" beam. Spectral windows 2 and 4 also contain a number of (thermal and maser) SiO and SiO isotopologue lines that can be imaged in full

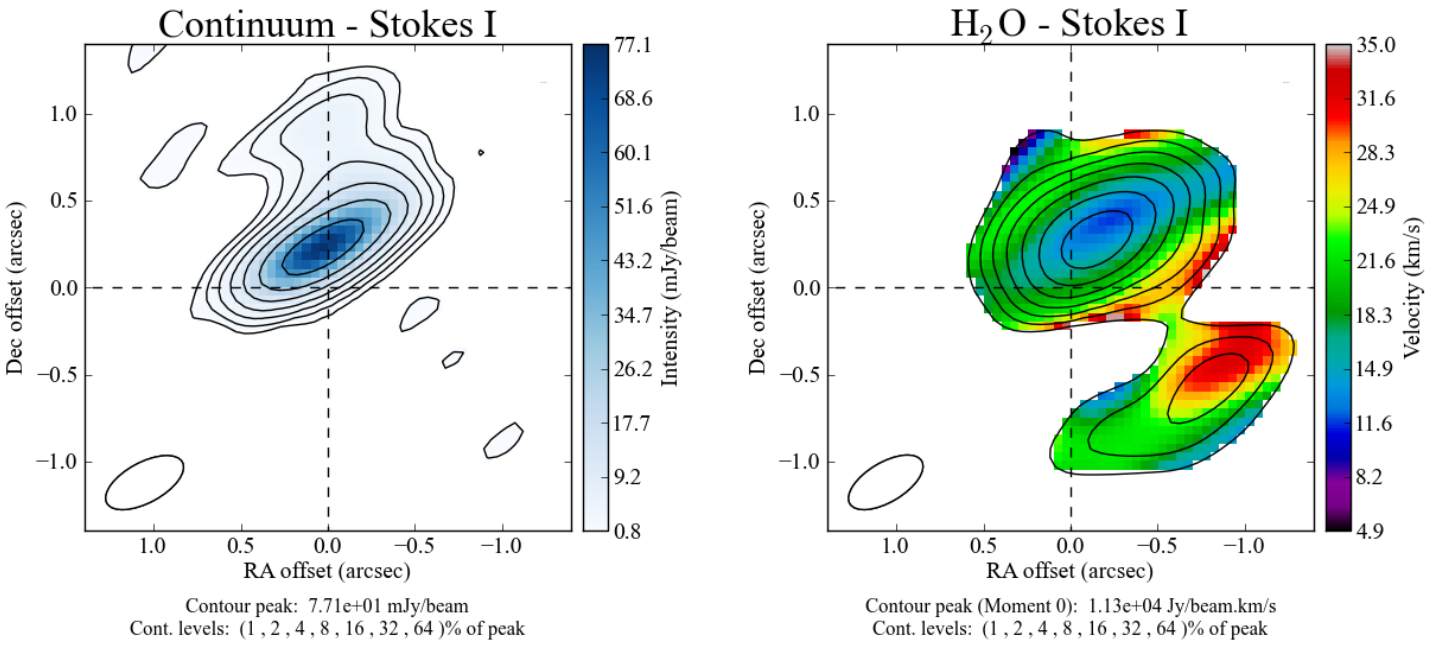

Figure 20: Band 5 continuum image of VY CMa (left) and H_2O maser moment 0 and 1 (right).

polarisation (not included in the reference images). Spectra of the masers are shown in Fig. 22.

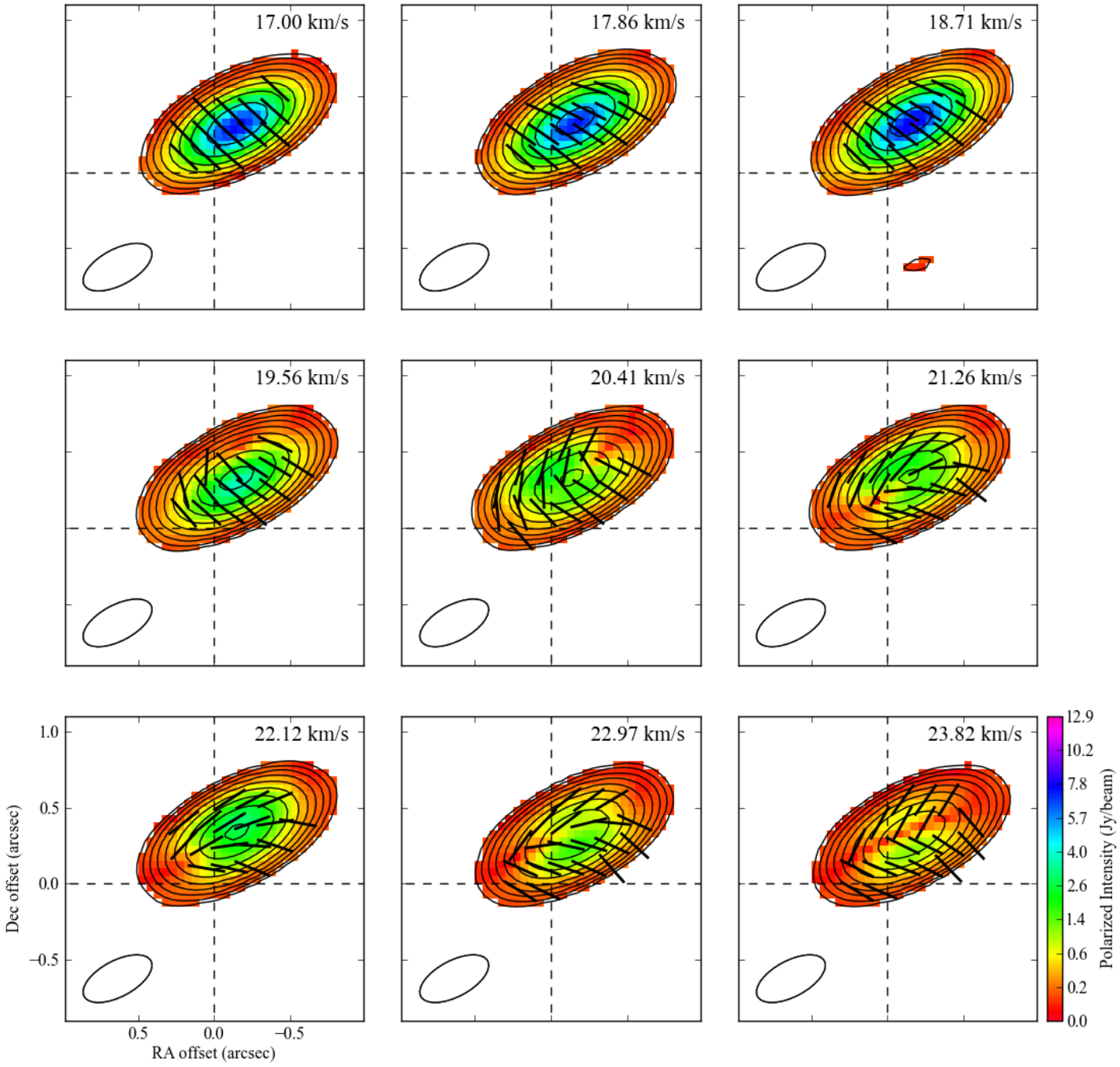

Figure 21: Channels maps of the full polarisation of the SiO masers at 172.5 GHz around VY CMa.

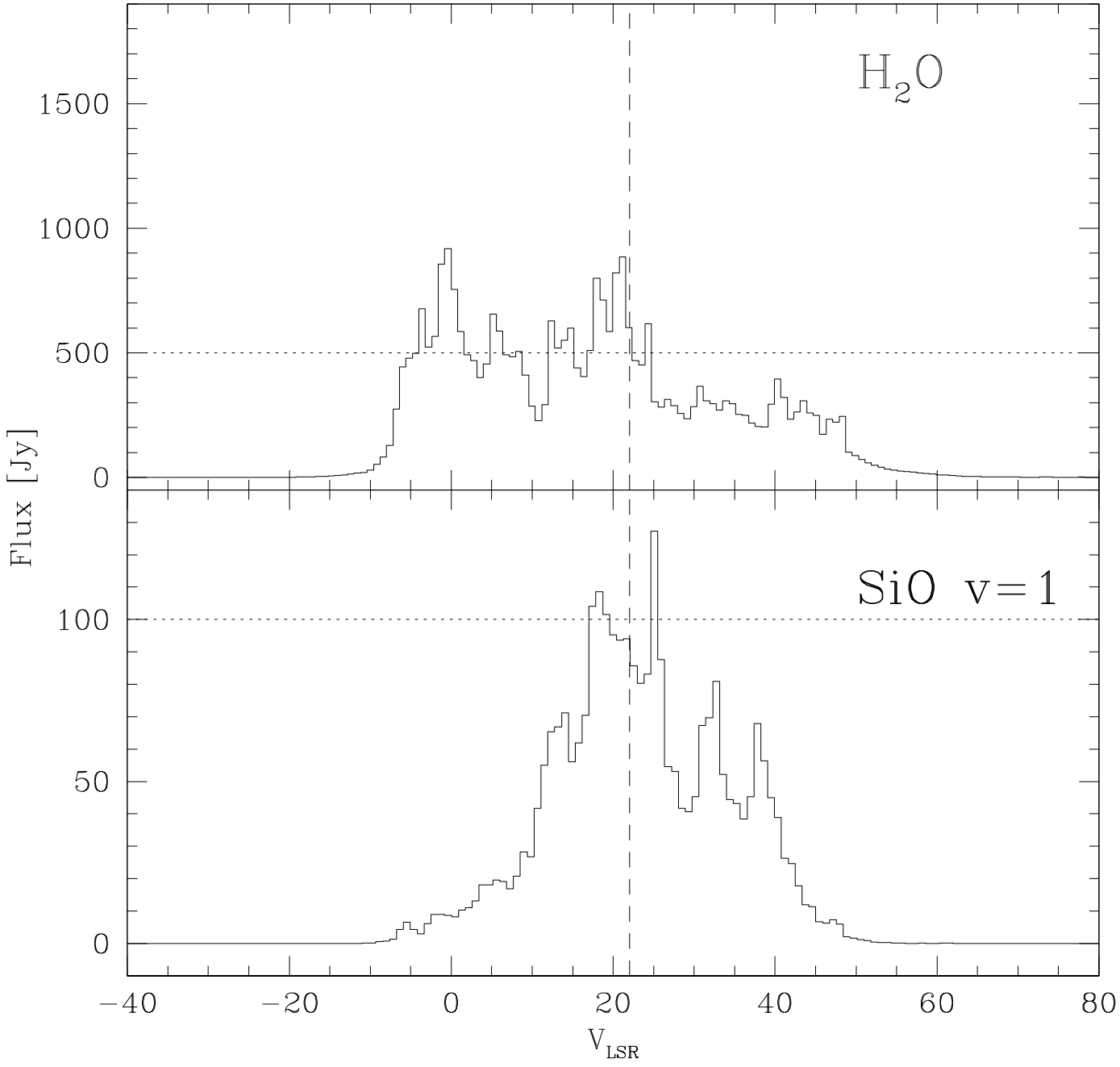

Figure 22: H_2O (top) and SiO (bottom) total intensity maser spectra. Vertical line denotes the stellar velocity, horizontal lines indicate preliminary APEX flux levels. Note the amplitude scaling in the atmospheric window of both APEX and ALMA is uncertain.